nanomaterials

MDPI

Article

Cluster Formation Effect of Water on Pristine and Defective MoS_2 Monolayers

Kangli Wang * and Beate Paulus *

Institut für Chemie und Biochemie, Freie Universität Berlin, Arnimallee 22, 14195 Berlin, Germany
* Correspondence: klwang0329@zedat.fu-berlin.de (K.W.); b.paulus@fu-berlin.de (B.P.)

Abstract: The structure and electronic properties of the molybdenum disulfide (MoS_2) monolayer upon water cluster adsorption are studied using density functional theory and the optical properties are further analyzed with the Bethe–Salpeter equation (BSE). Our results reveal that the water clusters are electron acceptors, and the acceptor tendency tends to increase with the size of the water cluster. The electronic band gap of both pristine and defective MoS_2 is rather insensitive to water cluster adsorbates, as all the clusters are weakly bound to the MoS_2 surface. However, our calculations on the BSE level show that the adsorption of the water cluster can dramatically redshift the optical absorption for both pristine and defective MoS_2 monolayers. The binding energy of the excitons of MoS_2 is greatly enhanced with the increasing size of the water cluster and finally converges to a value of approximately 1.16 eV and 1.09 eV for the pristine and defective MoS_2 monolayers, respectively. This illustrates that the presence of the water cluster could localize the excitons of MoS_2, thereby greatly enhance the excitonic binding energy.

Keywords: water cluster; molybdenum disulfide; optical properties; Bethe–Salpeter equation

check for updates

Citation: Wang, K.; Paulus, B. Cluster Formation Effect of Water on Pristine and Defective MoS_2 Monolayers. *Nanomaterials* **2023**, *13*, 229. https://doi.org/10.3390/nano13020229

Academic Editor: Antonio Di Bartolomeo

Received: 30 November 2022
Revised: 23 December 2022
Accepted: 27 December 2022
Published: 4 January 2023

Copyright: © 2023 by the authors. Licensee MDPI, Basel, Switzerland. This article is an open access article distributed under the terms and conditions of the Creative Commons Attribution (CC BY) license (https://creativecommons.org/licenses/by/4.0/).

1. Introduction

Recently, layered transition metal dichalcogenides (TMDs) have gained great attention due to their unusual electronic and optical properties, including sizable band gap, strong photoluminescence, excitonic effect, valley-specific circular dichroism, and so on [1–8]. For instance, while the bulk MoS_2 is an indirect band gap semiconductor, monolayer MoS_2 is a direct band gap semiconductor. Importantly, the exciton in the MoS_2 monolayer is strongly bound because of the reduced dimensionality. The presence of intrinsic structural defects in TMDs [9–11], which is inevitable in the experiments, provides even more possibility to tune the reactivity and transport properties and create new functionalities. For example, NO molecules can chemically adsorb on the sulfur (S) defects of the MoS_2 monolayer [12–14], indicating the high sensitivity towards NO molecules and the great potential of TMDs as gas sensors. These suggest that the layered TMDs, in particular MoS_2, are promising candidates for graphene replacement with various application possibilities.

In reality, the humidity, i.e., the effect of adsorption of water, plays an important role in countless applications and technological processes, since water is present in the environment of almost any device. Examples include field-effect transistors [15], gas sensors [16,17], and electronic devices [18]. In addition, various water clusters $(H_2O)_n$ can form via intermolecular hydrogen bonds on the surface of a solid depending on the environmental conditions [19–26]. Therefore, the understanding of the properties of water/solid interface is very important for the development and improvement of various applications.

The great potential of the MoS_2 monolayer and the importance of the water/solid interface call for a theoretical perspective on how the presence of water influences the electronic and optical properties of MoS_2. A single water molecule was theoretically predicted to only weakly adsorb on the MoS_2 surface compared with other inorganic molecules, and had no influence on the electronic band gap [12,13,27–30]. However, there

is still a lack of theoretical understanding of the influence of a single water molecule on the optical and excitonic properties. More importantly, the effect of water clusters associated with hydrogen bonds on the electronic and optical properties of the MoS_2 monolayer is still largely unexplored.

It is well known that the GW approximation combined with the Bethe–Salpeter equation based on DFT (DFT-GW-BSE) [31–33] can accurately model photoemission measurements and optical absorption. In this work, by employing this method, we analyze how the water cluster influences the electronic, optical and excitonic properties of both pristine and defective MoS_2 monolayers. In this model, a water cluster consisting of up to five water molecules is considered to adsorb on a large supercell of the MoS_2 monolayer.

2. Computational Details

All calculations except for the charge density difference are performed using GPAW code [34] based on the projector augmented wave method. To describe the exchange and correlation effects, including the dispersion interaction, we adopt the vdW-DF-CX functional [35] to obtain the structures upon water cluster adsorption. A cutoff energy of 500 eV for the plane-wave basis set and a Monkhorst–Pack k-point sampling of $6 \times 6 \times 1$ are employed. The S defect is the main factor among the intrinsic structural defects in TMDs. Therefore, in order to ensure that the S defect density in our simulation models is in the same magnitude of experimental density (10^{13} cm^{-2}) [9,36], one S defect is created in a (4×4) supercell of the MoS_2 monolayer, corresponding to a defect density of 6.2×10^{13} cm^{-2}. A vacuum space of more than 15 Å is chosen during geometry optimization to avoid undesired interactions between neighboring supercells in the perpendicular direction. The clusters containing up to five water molecules are considered to absorb on the MoS_2 surface. All the structures are fully relaxed until the maximum force acting on each atom is less than 0.02 eV/Å and the energy change is less than 10^{-5} eV. Within this frame, we obtain a lattice constant of 3.18 Å and a Mo-S bond length of 2.41 Å for the pristine MoS_2, which are in good agreement with experimental results [37] and previous simulations [38,39]. Using the optimized structures, the charge transfer between adsorbate and substrate is discussed by means of Bader analysis [40]. The charge density calculation is performed by means of the DFT method at the vdW-DF-CX level using the plane wave Vienna ab initio Simulation Package (VASP) code [41,42] and the same computational parameters as for the GPAW calculations.

The DFT-GW-BSE method is a three-step procedure to determine the electronic and optical properties of a solid. The first step is to obtain the Kohn–Sham energies and wave functions by DFT calculation. In the second step, the quasi-particle (QP) band structure energies are obtained by GW approximation. Finally, the BSE is solved to get the coupled electron–hole excitation energies and exciton wave functions. Motivated by the weak interaction between adsorbate and substrate and the high cost of GW calculation, we use an approximated method, DFT-*app*G_0W_0-BSE (one-shot G_0W_0: GW equations are not solved self-consistently), to perform the BSE calculation. In this method, the electron–hole interaction is approximated by applying the scissor operator to the DFT band structure of the adsorbate/substrate system according to the QP band gap of the substrate (as displayed in Figure 1), motivated by the negligible influence of the adsorbate on the electron–hole interaction in a certain range. To enable a more direct comparison with DFT-GW-BSE, we apply the DFT-G_0W_0-BSE and DFT-*app*G_0W_0-BSE methods to the case of a single H_2O molecule on the pristine MoS_2 unit cell. The corresponding results are displayed in Figure 2. It is clear that the optical absorption spectrum calculated by the DFT-*app*G_0W_0-BSE method is in good agreement with that by the DFT-G_0W_0-BSE method within 0.05 eV deviation.

After successfully applying the DFT-*app*G_0W_0-BSE method to describe the optical properties of a single H_2O molecule on the pristine MoS_2 unit cell, we extend our investigation to the optical properties of the water cluster on a (4×4) supercell. The DFT calculation is performed by the general gradient approximation along with the Perdew–Burke–Ernzerhof (PBE) exchange–correlation functional [43]. Our previous study [39] shows that for a (4×4)

supercell, 10 Å vacuum with 50 eV G_0W_0 self-energy and $3 \times 3 \times 1$ k-point sampling is sufficient to obtain the converged QP band gap by employing the 2D truncation. Therefore, the same parameters are applied to the G_0W_0 calculation of the pristine and defective MoS_2. To obtain converged optical spectra, the 16 highest valence bands and the 32 lowest conduction bands are used as a basis to calculate excitonic contribution with a large k-point grid of $8 \times 8 \times 1$. The spectrum is obtained by applying a Lorentzian broadening with a fullwidth half maximum of 0.05 eV.

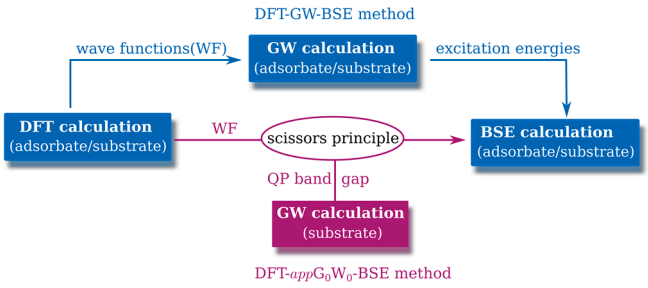

Figure 1. Schematic illustration of DFT-GW-BSE [31–33] and DFT-*app*G_0W0-BSE.

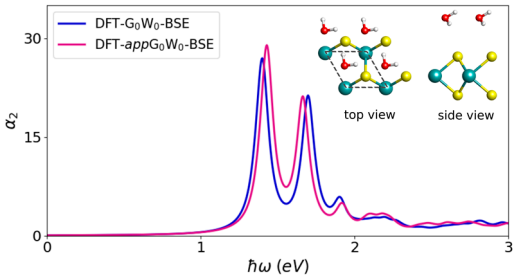

Figure 2. Optical absorption spectra for MoS_2 with one H_2O molecule in a unit cell by DFT-G_0W_0-BSE and DFT-*app*G_0W_0-BSE methods with PBE functional. The spectra are obtained by applying a Lorentzian broadening of 0.05 eV. For both cases, the electronic band gap is 2.48 eV. The corresponding structure is also shown.

3. Results

3.1. Configurations of $(H_2O)_n$ on MoS_2 Monolayers

We first investigate the adsorption of $(H_2O)_n$ on both pristine and defective MoS_2 surfaces by identifying the most stable adsorption structures. Various high-symmetry adsorption sites and adsorption orientations are considered; the most favorable configurations and corresponding results are presented in Figure 3 and Table 1, respectively. We discriminate between the adsorption energy of the whole cluster on MoS_2 and the binding energy, which is referred to the isolated water molecules. The adsorption energy is calculated as

$$E_{ad} = E_{tot} - E_{MoS_2} - E_{cluster} \quad (1)$$

where E_{tot} represents the total energy of MoS_2 with cluster adsorbed, E_{MoS_2} and $E_{cluster}$ are the energies of the MoS_2 monolayer and the isolated cluster. The binding energy is determined using

$$E_{bind} = E_{tot} - E_{MoS_2} - nE_{H_2O} \quad (2)$$

where E_{tot}, E_{MoS_2}, E_{H_2O}, and n are the total energy of MoS_2 with the cluster adsorbed, the energy of the MoS_2 monolayer, the energy of relaxed H_2O molecule, and the number of H_2O molecules in the cluster, respectively. As shown in Figure 3, for the pristine surface, the monomer H_2O is preferably adsorbed at the hollow site, with two O-H bonds orienting towards the monolayer. In the case of the dimer, trimer, tetramer, and pentamer, water clusters prefer to form the linear, triangular, quadrilateral, and pentagonal shapes on the surface of MoS_2, respectively. In particular, we observe that a ring trimer is more stable than an open structure on the MoS_2 surface, which differs from that on the Pt(111)

surface [44]. In addition, due to the cluster–surface interaction, these water clusters tend to lie on the pristine surface. Generally speaking, the shape and orientation of water clusters on the pristine MoS_2 surface are almost identical to the gas-phase of water clusters [45–48]. As displayed in Table 1, the binding energy of water clusters on the pristine surface dramatically increases with the increasing size of the cluster as more hydrogen bonds form within the cluster. We also note that the hydrogen bonds in the cluster become stronger with the size of the water cluster, e.g., trimer: 0.23 eV, tetramer: 0.31 eV, and pentamer: 0.33 eV. This is because the angular strain becomes smaller in a large water cluster. In comparison with the adsorption energy, the binding energy has a larger negative value since it contains contributions from the intermolecular hydrogen bonding in addition to the cluster–surface interaction. Both binding and adsorption energies show that the water cluster binds stronger to the MoS_2 surface than monomer water, indicating the tendency towards larger water clusters on the MoS_2 surface. In general, the water clusters are weakly bound to the pristine MoS_2 with a large separation bigger than 2.98 Å between them.

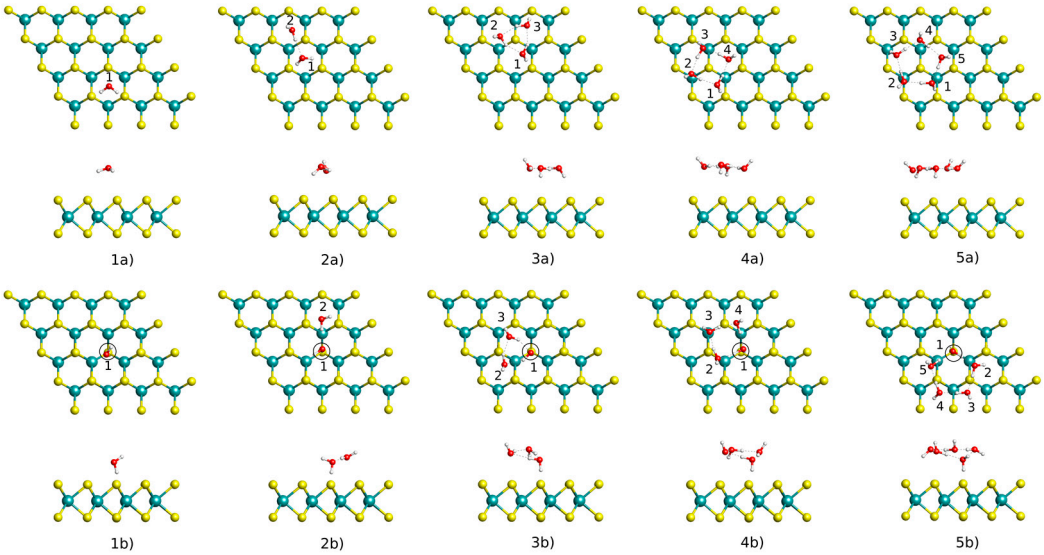

Figure 3. The most favorable configurations for $(H_2O)_n$ (n = 1–5) on the pristine and defective MoS_2 monolayers obtained by geometry optimization with the vdW-DF-CX functional. The notations of (**1a**–**5a**) and (**1b**–**5b**) correspond to the pristine and defective surface, respectively; numbers 1–5 correspond to the number of water molecules on the surface. The S defect is represented by the black circle.

Table 1. The binding energy (E_{bind}), adsorption energy (E_{ad}), and equilibrium height (h) between the center of mass of the molecule and the top S-layer, total charge transfer (ΔQ) from MoS_2 to water cluster, and individual charge.

No. [a]	E_{bind}(eV)	E_{ad}(eV)	h(Å)	ΔQ(e) [b]	Individual ΔQ(e)				
					$H_2O(1)$ [c]	$H_2O(2)$ [c]	$H_2O(3)$ [c]	$H_2O(4)$ [c]	$H_2O(5)$ [c]
1a)	−0.140	−0.140	2.976	0.006	0.006				
2a)	−0.488	−0.273	2.866	0.017	−0.005	0.022			
3a)	−0.990	−0.308	3.110	0.025	0.010	0.000	0.015		
4a)	−1.649	−0.402	3.193	0.022	0.008	0.001	0.012	0.001	
5a)	−2.127	−0.486	3.177	0.020	0.011	0.002	0.007	−0.003	0.003
1b)	−0.209	−0.209	2.082	0.032	0.032				
2b)	−0.537	−0.322	2.385	0.025	0.018	0.007			
3b)	−1.029	−0.347	2.849	0.032	0.023	0.004	0.005		
4b)	−1.663	−0.416	2.976	0.033	0.026	0.001	0.006	0.001	
5b)	−2.178	−0.537	3.061	0.031	0.022	0.004	−0.003	0.007	0.001

[a] The numbering notations correspond to the structures presented in Figure 3. [b] The sign of the charge transfer value indicates the direction. [c] The numbering notations correspond to the water molecules presented in Figure 3.

For the defective surface, we find that the monomer water adopts a vertical configuration with one O-H bond pointing towards the defect, which is in good agreement with the previous calculations [12]. When the dimer, trimer, tetramer, and pentamer adsorb on the defective MoS_2 surface, the structure of the water clusters changes as influenced by hydrogen bonding and cluster–defect interactions. Therefore, one molecule of the water cluster is always adsorbed at the defect with a small separation. The adsorption energy of water clusters on the defective surface (in range of −0.21 eV to −0.54 eV) is slightly larger than that on the pristine surface (in range of −0.14 to −0.49 eV), implying that the defect is a center of adsorption. Although the adsorption energy and distance between the water cluster and MoS_2 monolayer are greatly influenced by the presence of the defect, all these water clusters are only physisorbed on the defective MoS_2.

3.2. Electronic Properties

Figure 4 and Table 1 display how the electron density rearranges upon the adsorption of the water clusters. The corresponding charge density difference is calculated by the formula $\Delta\rho = \rho_{tot} - \rho_{MoS_2} - \rho_{cluster}$, where ρ_{tot}, ρ_{MoS_2} and $\rho_{cluster}$ are the charge density of the MoS_2 with adsorption, MoS_2 monolayer, and isolated cluster, respectively. It is shown that for both pristine and defective MoS_2, the oxygen atom in the water gains charge density, while the hydrogens lose charge density, resulting in a small number of electrons to be transferred from MoS_2 to the water cluster. It also implies that the charge rearrangement between MoS_2 and the water cluster depends on the orientation of the water molecule. For example, when a water dimer is adsorbed on the pristine surface, 0.022 e is transferred from the MoS_2 to one water molecule (labeled as $H_2O(2)$ in Table 1); while 0.005 e is transferred to the MoS_2 from the other water molecule (labeled as $H_2O(1)$ in Table 1). The charge rearrangement mainly occurs on the S atoms and partly on the Mo atoms of MoS_2 around each absorption site. As the water cluster grows, the charge transfer between the water cluster and host tends to converge for both pristine and defective surfaces. Compared with the pristine surface, a larger charge transfer occurs between the water cluster and the defective MoS_2, also reflected by their stronger adsorption as described above. As revealed by Table 1, up to 0.033 e is transferred from the defective MoS_2 to the water cluster. The transferred electrons are mainly distributed in the water molecule adsorbed at the S defect (labeled as $H_2O(1)$). This behavior arises from the presence of the unsaturated Mo atom on the surface, which leaves excess electrons at the S defect. We can conclude overall from this analysis that the water clusters acting as electron acceptors induce charge redistribution for both pristine and defective MoS_2 hosts.

We next examine the band structure and DOS (see Supporting Information) of the water cluster adsorbing on both pristine and defective MoS_2 surfaces. Since the DFT method always underestimates the band gap, the G_0W_0 calculation is performed for the pristine and defective MoS_2. For the pristine MoS_2 monolayer, our G_0W_0 band gap of 2.55 eV is slightly larger than our previous result of 2.49 eV, mainly due to the exclusion of spin–orbit interaction in the present work. We find that the spin–orbit splitting calculated by G_0W_0 is almost the same as vdW-DF-CX. Therefore, after including the spin–orbit splitting from the DFT method at the vdW-DF-CX level, the calculated band gap of 2.48 eV of the pristine MoS_2 monolayer agrees well with the experimental values of approximately 2.5 eV [49]. The presence of an S defect on the MoS_2 induces three localized states in the band gap: two unoccupied states around 1.58 eV and one occupied state around −0.42 eV (see Figure S1 in Supporting Information). In addition, the unoccupied states undergo a spin–orbit splitting of 0.05 eV at the K point, giving rise to a QP band gap of 1.95 eV. Concerning the adsorption of the water clusters, our DFT band structure and DOS calculation show that the molecular states are present deeply in the valence band and conduction band of MoS_2 and hybrids with host states, implying that the band gap of MoS_2 is insensitive towards perturbations by the water clusters. Thus, the G_0W_0 calculation will not be performed upon the adsorption of the water clusters.

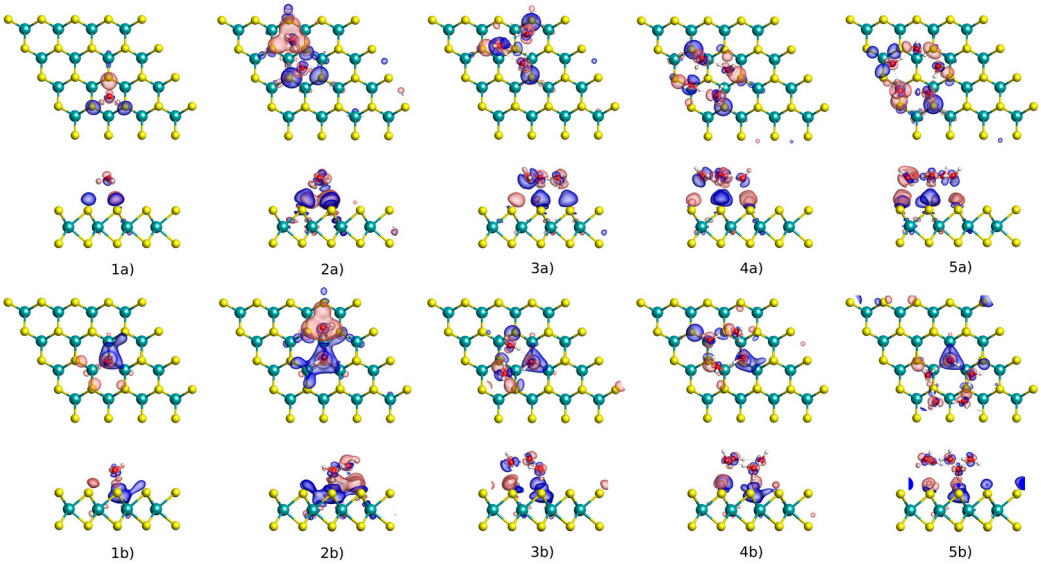

Figure 4. Charge density difference plots for $(H_2O)_n$ (n = 1–5) on the pristine and defective MoS_2 monolayers by vdW-DF-cx functional. The notations of (**1a**–**5a**) and (**1b**–**5b**) correspond to the pristine and defective surfaces, respectively; numbers 1–5 correspond to the number of water molecules on the surface. The red (blue) distribution corresponds to charge accumulation (depletion). The isosurface value of 0.005 $e^-/Bohr^3$ is considered for all the cases.

3.3. Optical and Excitonic Properties

We proceed to investigate the optical properties of $(H_2O)_n/MoS_2$ by solving the BSE equations. Figure 5 depicts the optical absorption spectra with and without the adsorption of water clusters on the MoS_2 monolayer, and the corresponding results are summarized in Table 2. The calculated optical band gap of 1.89 eV for the pristine MoS_2 monolayer is in excellent agreement with the experimental value of approximately 1.9 eV [6,49]. As a result, the corresponding excitonic binding energy of 0.59 eV is obtained in this work. The sharp peaks A and B are located at 1.89 eV and 2.02 eV, respectively, associating with the direct transitions from the spin–orbit split valence band to the conduction bands at the K point in the Brillouin zone. The adsorption of the monomer water on the pristine MoS_2 dramatically redshifts the absorption edge of the optical spectrum and induces an absorption shoulder at 1.64 eV, corresponding to a strongly bound exciton with 0.84 eV binding energy. It is well known that the excitons in 2D-TMDs are of the Wannier–Mott type and thus delocalized in space [50]. A localized exciton with strong electron–hole interaction is observed upon the adsorption of the water cluster. In addition, as the water cluster grows, the optical absorption peak is shifted to lower energy and the binding energy of excitons becomes larger, and both of them finally converge to a value of approximately 1.32 eV and 1.17 eV, respectively. This convergence indicates that the exciton binding energy may be insensitive to further growth of the water cluster. More interestingly, the optical absorption is greatly strengthened in the spectral range of 1.5–2.5 eV. The enhanced optical absorption is attributed to the charge transfer between the water cluster and host which depletes the n-type conductivity in MoS_2 and further reduces the electrostatic screening [51,52].

In comparison with the pristine MoS_2, the presence of an S defect greatly redshifts the first absorption peak to 1.32 eV with attenuated intensity. The excitonic binding energy with 0.63 eV is slightly stronger than that of the pristine MoS_2. This is because the unsaturated Mo atom leaves excess electrons at the S defect, leading to the formation of the charged exciton. The adsorption of the water clusters on the defective surface also redshifts the optical absorption edge compared with that on the pristine MoS_2, but the optical band gap converges to a smaller value of approximately 0.86 eV with the increasing size of the water cluster. Thus, the binding energy of the charged exciton converges to a value of approximately 1.09 eV with the increasing size of the water cluster. Although the first optical absorption peak is weakened

by the adsorption of the water clusters, the optical absorption between 1.5 and 2.0 eV is greatly strengthened as similarly observed for the pristine MoS_2 series. In conclusion, the optical absorption of both pristine and defective MoS_2 can be redshifted and is further enhanced in the infrared region by water clusters adsorption.

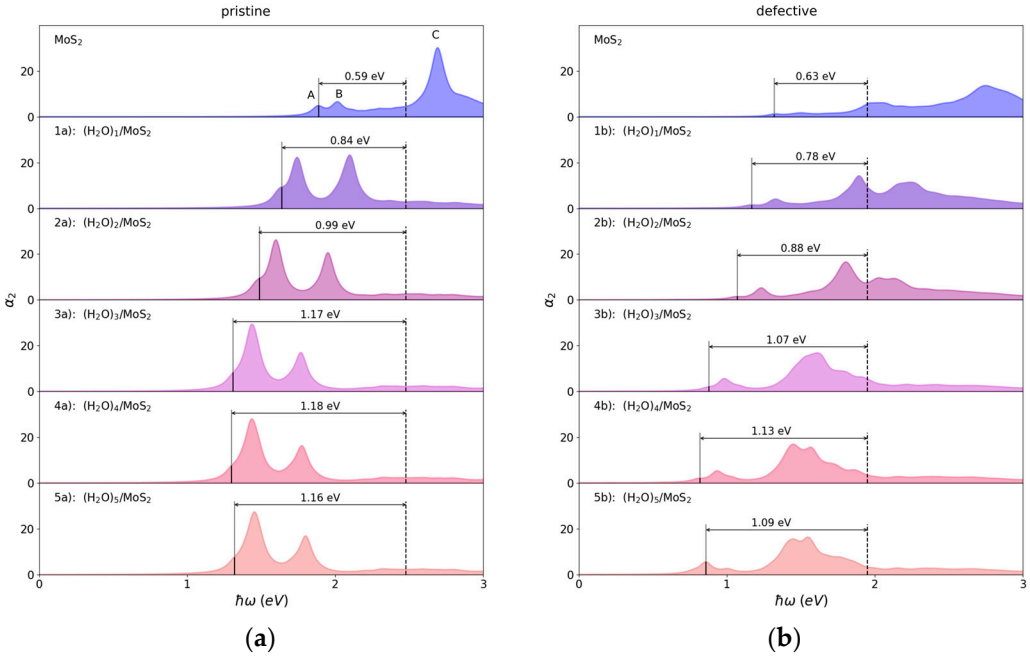

Figure 5. The optical absorption spectra for $(H_2O)_n$ (n = 1–5) on the pristine and defective MoS_2 monolayers simulated with the DFT-*app*G_0W_0-BSE method. The dark solid and dashed lines indicate the optical and electronic band gap, respectively. Excitonic binding energies are shown as well. The notations of A, B and C correspond to the optical absorption peaks. The notations of (**a**) and (**b**) correspond to the pristine and defective surfaces, respectively; numbers 1–5 correspond to the number of water molecules on the surface.

Table 2. The QP electronic band gap (E_{ele}), optical band gap (E_{opt}), and excitonic binding energy (E_{ext}) for $(H_2O)_n$ (n = 1–5) on the pristine and defective MoS_2 monolayers.

No.	E_{ele}(eV)	E_{opt}(eV)	E_{ext}(eV)
pristine MoS_2	2.48	1.89	0.59
1a)	2.48	1.64	0.84
2a)	2.48	1.49	0.99
3a)	2.48	1.31	1.17
4a)	2.48	1.3	1.18
5a)	2.48	1.32	1.16
defective MoS_2	1.95	1.32	0.63
1b)	1.95	1.17	0.78
2b)	1.95	1.07	0.88
3b)	1.95	0.88	1.07
4b)	1.95	0.82	1.13
5b)	1.95	0.86	1.09

4. Conclusions

In summary, by employing the DFT-*app*G_0W_0-BSE method, we explored how the electronic and optical properties of the MoS_2 monolayer are affected by the adsorption of water

clusters of different sizes. It was found that (1) the water clusters $(H_2O)_n$ (n = 1–5) have weak interaction with both pristine and defective MoS_2 monolayers, (2) no additional states are introduced in the gap region of both pristine and defective MoS_2 by the adsorption of the water clusters; and (3) the presence of the water clusters can dramatically redshift the optical absorption for both pristine and defective MoS_2 monolayers.

Supplementary Materials: The following supporting information can be downloaded at: https://www.mdpi.com/article/10.3390/nano13020229/s1, Figure S1: electronic band structure for the pristine and defective MoS_2 monolayers; Figures S2 and S3: electronic band structure for $(H_2O)_n$ (n = 1–5) on the pristine and defective MoS_2 monolayers, respectively; Figure S4: total density of states and the projected density of states for $(H_2O)_n$ (n = 1–5) on pristine and defective MoS_2; optimized geometries considered in this work.

Author Contributions: Conceptualization, B.P. and K.W.; formal analysis, K.W.; funding acquisition, B.P. and K.W.; investigation, K.W.; resources, B.P. and K.W.; supervision, B.P.; validation, K.W.; visualization, K.W.; writing—original draft, K.W.; writing—review and editing, K.W. and B.P. All authors have read and agreed to the published version of the manuscript.

Funding: This research received no external funding. The publication of this article was funded by Freie Universität Berlin.

Institutional Review Board Statement: Not applicable.

Informed Consent Statement: Not applicable.

Data Availability Statement: Not applicable.

Acknowledgments: K.W. acknowledges the China Scholarship Council for the financial support. B.P. and K.W. thank Kirill Bolotin for the fruitful discussions. The computations were performed with resources provided by the North-German Supercomputing Alliance (HLRN) and computer facilities of the Freie Universitäte Berlin (ZEDAT).

Conflicts of Interest: The authors have no conflict to declare.

References

1. Gusakova, J.; Wang, X.; Shiau, L.L.; Krivosheeva, A.; Shaposhnikov, V.; Borisenko, V.; Gusakov, V.; Tay, B.K. Electronic Properties of Bulk and Monolayer TMDs: Theoretical Study Within DFT Framework (GVJ-2e Method). *Phys. Status Solidi A* **2017**, *214*, 1700218. [CrossRef]
2. Kylänpää, I.; Komsa, H.-P. Binding energies of exciton complexes in transition metal dichalcogenide monolayers and effect of dielectric environment. *Phys. Rev. B* **2015**, *92*, 205418. [CrossRef]
3. Berghäuser, G.; Malic, E. Analytical approach to excitonic properties of MoS_2. *Phys. Rev. B* **2014**, *89*, 125309. [CrossRef]
4. Ramasubramaniam, A. Large excitonic effects in monolayers of molybdenum and tungsten dichalcogenides. *Phys. Rev. B* **2012**, *86*, 115409. [CrossRef]
5. He, K.; Kumar, N.; Zhao, L.; Wang, Z.; Mak, K.F.; Zhao, H.; Shan, J. Tightly Bound Excitons in Monolayer WSe_2. *Phys. Rev. Lett.* **2014**, *113*, 026803. [CrossRef] [PubMed]
6. Mak, K.F.; Lee, C.; Hone, J.; Shan, J.; Heinz, T.F. Atomically Thin MoS_2: A New Direct-Gap Semiconductor. *Phys. Rev. Lett.* **2010**, *105*, 136805. [CrossRef]
7. Mak, K.F.; He, K.; Shan, J.; Heinz, T.F. Control of valley polarization in monolayer MoS_2 by optical helicity. *Nat. Nanotechnol.* **2012**, *7*, 494–498. [CrossRef] [PubMed]
8. Splendiani, A.; Sun, L.; Zhang, Y.; Li, T.; Kim, J.; Chim, C.-Y.; Galli, G.; Wang, F. Emerging Photoluminescence in Monolayer MoS_2. *Nano Lett.* **2010**, *10*, 1271–1275. [CrossRef]
9. Hong, J.; Hu, Z.; Probert, M.; Li, K.; Lv, D.; Yang, X.; Gu, L.; Mao, N.; Feng, Q.; Xie, L.; et al. Exploring atomic defects in molybdenum disulphide monolayers. *Nat. Commun.* **2015**, *6*, 6293. [CrossRef]
10. Zhou, W.; Zou, X.; Najmaei, S.; Liu, Z.; Shi, Y.; Kong, J.; Lou, J.; Ajayan, P.M.; Yakobson, B.I.; Idrobo, J.-C. Intrinsic structural defects in monolayer molybdenum disulfide. *Nano Lett.* **2013**, *13*, 2615–2622. [CrossRef]
11. Stampfer, B.; Zhang, F.; Illarionov, Y.Y.; Knobloch, T.; Wu, P.; Waltl, M.; Grill, A.; Appenzeller, J.; Grasser, T. Characterization of Single Defects in Ultrascaled MoS_2 Field-Effect Transistors. *ACS Nano* **2018**, *12*, 5368–5375. [CrossRef] [PubMed]
12. Li, H.; Huang, M.; Cao, G. Markedly different adsorption behaviors of gas molecules on defective monolayer MoS2: A first-principles study. *Phys. Chem. Chem. Phys.* **2016**, *18*, 15110–15117. [CrossRef] [PubMed]
13. González, C.; Biel, B.; Dappe, Y.J. Adsorption of small inorganic molecules on a defective MoS_2 monolayer. *Phys. Chem. Chem. Phys.* **2017**, *19*, 9485–9499. [CrossRef] [PubMed]

14. Li, F.; Shi, C. NO-sensing performance of vacancy defective monolayer MoS_2 predicted by density function theory. *Appl. Surf. Sci.* **2017**, *434*, 294–306. [CrossRef]
15. Lowe, B.M.; Maekawa, Y.; Shibuta, Y.; Sakata, T.; Skylaris, C.-K.; Green, N.G. Dynamic behaviour of the silica-water-bio electrical double layer in the presence of a divalent electrolyte. *Phys. Chem. Chem. Phys.* **2017**, *19*, 2687–2701. [CrossRef]
16. Kokabu, T.; Inoue, S.; Matsumura, Y. Effect of molecular coverage on the electric conductance of a multi-walled carbon nanotube thin film. *Chem. Phys. Lett.* **2016**, *654*, 9–12. [CrossRef]
17. Kokabu, T.; Takashima, K.; Inoue, S.; Matsumura, Y.; Yamamoto, T. Transport phenomena of electrons at the carbon nanotube interface with molecular adsorption. *J. Appl. Phys.* **2017**, *122*, 015308. [CrossRef]
18. Melios, C.; Giusca, C.E.; Panchal, V.; Kazakova, O. Water on graphene: Review of recent progress. *2D Mater.* **2018**, *5*, 022001. [CrossRef]
19. Thiel, P.A.; Madey, T.E. The interaction of water with solid surfaces: Fundamental aspects. *Surf. Sci. Rep.* **1987**, *7*, 211–385. [CrossRef]
20. Henderson, M.A. The interaction of water with solid surfaces: Fundamental aspects revisited. *Surf. Sci. Rep.* **2002**, *46*, 1–308. [CrossRef]
21. Hodgson, A.; Haq, S. Water adsorption and the wetting of metal surfaces. *Surf. Sci. Rep.* **2009**, *64*, 381–451. [CrossRef]
22. Carrasco, J.; Hodgson, A.; Michaelides, A. A molecular perspective of water at metal interfaces. *Nat. Mater.* **2012**, *11*, 667–674. [CrossRef] [PubMed]
23. Mitsui, T.; Rose, M.K.; Fomin, E.; Ogletree, D.F.; Salmeron, M. Water Diffusion and Clustering on Pd(111). *Science* **2002**, *297*, 1850–1852. [CrossRef] [PubMed]
24. Dong, A.; Yan, L.; Sun, L.; Yan, S.; Shan, X.; Guo, Y.; Meng, S.; Lu, X. Identifying Few Molecule Water Clusters with High Precision on Au(111) Surface. *ACS Nano* **2018**, *12*, 6452–6457. [CrossRef] [PubMed]
25. Tatarkhanov, M.; Ogletree, D.F.; Rose, F.; Mitsui, T.; Fomin, E.; Maier, S.; Rose, M.; Cerdá, J.I.; Salmeron, M. Metal- and Hydrogen-Bonding Competition during Water Adsorption on Pd(111) and Ru(0001). *J. Am. Chem. Soc.* **2009**, *131*, 18425–18434. [CrossRef] [PubMed]
26. Drüppel, M.; Deilmann, T.; Krüger, P.; Rohlfing, M. Diversity of trion states and substrate effects in the optical properties of an MoS_2 monolayer. *Nat. Commun.* **2017**, *8*, 2117. [CrossRef]
27. Yue, Q.; Shao, Z.; Chang, S.; Li, J. Adsorption of gas molecules on monolayer MoS_2 and effect of applied electric field. *Nanoscale Res. Lett.* **2013**, *8*, 425. [CrossRef]
28. Zhao, S.; Xue, J.; Kang, W. Gas adsorption on MoS_2 monolayer from first-principles calculations. *Chem. Phys. Lett.* **2014**, *595*, 35–42. [CrossRef]
29. Ferreira, F.; Carvalho, A.; Moura, Í.J.M.; Coutinho, J.; Ribeiro, R.M. Adsorption of H_2, O_2, H_2O, OH and H on monolayer MoS_2. *J. Phys. Condens. Matter* **2018**, *30*, 035003. [CrossRef]
30. Levita, G.; Restuccia, P.; Righi, M.C. Graphene and MoS_2 interacting with water: A comparison by ab initio calculations. *Carbon* **2016**, *107*, 878–884. [CrossRef]
31. Hybertsen, M.S.; Louie, S.G. Electron correlation in semiconductors and insulators: Band gaps and quasiparticle energies. *Phys. Rev. B* **1986**, *34*, 5390–5413. [CrossRef] [PubMed]
32. Rohlfing, M.; Louie, S.G. Electron-Hole Excitations in Semiconductors and Insulators. *Phys. Rev. Lett.* **1998**, *81*, 2312–2315. [CrossRef]
33. Benedict, L.X.; Shirley, E.L.; Bohn, R.B. Optical Absorption of Insulators and the Electron-Hole Interaction: An Ab Initio Calculation. *Phys. Rev. Lett.* **1998**, *80*, 4514–4517. [CrossRef]
34. Enkovaara, J.; Rostgaard, C.; Mortensen, J.J.; Chen, J.; Dułak, M.; Ferrighi, L.; Gavnholt, J.; Glinsvad, C.; Haikola, V.; Hansen, H.A.; et al. Electronic structure calculations with GPAW: A real-space implementation of the projector augmented-wave method. *J. Phys. Condens. Matter* **2010**, *22*, 253202. [CrossRef]
35. Berland, K.; Hyldgaard, P. Exchange functional that tests the robustness of the plasmon description of the van der Waals density functional. *Phys. Rev. B* **2014**, *89*, 035412. [CrossRef]
36. Qiu, H.; Xu, T.; Wang, Z.; Ren, W.; Nan, H.; Ni, Z.; Chen, Q.; Yuan, S.; Miao, F.; Song, F.; et al. Hopping transport through defect-induced localized states in molybdenum disulphide. *Nat. Commun.* **2013**, *4*, 2642. [CrossRef]
37. Wilson, J.A.; Yoffe, A.D. The transition metal dichalcogenides discussion and interpretation of the observed optical, electrical and structural properties. *Adv. Phys.* **1969**, *18*, 193–335. [CrossRef]
38. Rasmussen, F.A.; Thygesen, K.S. Computational 2D Materials Database: Electronic Structure of Transition-Metal Dichalcogenides and Oxides. *J. Phys. Chem. C* **2015**, *119*, 13169–13183. [CrossRef]
39. Wang, K.; Paulus, B. Tuning the binding energy of excitons in the MoS_2 monolayer by molecular functionalization and defective engineering. *Phys. Chem. Chem. Phys.* **2020**, *22*, 11936–11942. [CrossRef]
40. Tang, W.; Sanville, E.; Henkelman, G. A grid-based Bader analysis algorithm without lattice bias. *J. Phys. Condens. Matter* **2009**, *21*, 084204. [CrossRef]
41. Kresse, G.; Hafner, J. Ab initio molecular dynamics for liquid metals. *Phys. Rev. B* **1993**, *47*, 558–561. [CrossRef] [PubMed]
42. Kresse, G.; Furthmüller, J. Efficient iterative schemes for ab initio total-energy calculations using a plane-wave basis set. *Phys. Rev. B* **1996**, *54*, 11169–11186. [CrossRef] [PubMed]

43. Perdew, J.P.; Burke, K.; Ernzerhof, M. Generalized Gradient Approximation Made Simple. *Phys. Rev. Lett.* **1996**, *77*, 3865–3868. [CrossRef] [PubMed]
44. Árnadóttir, L.; Stuve, E.M.; Jónsson, H. Adsorption of water monomer and clusters on platinum(111) terrace and related steps and kinks: I. Configurations, energies, and hydrogen bonding. *Surf. Sci.* **2010**, *604*, 1978–1986. [CrossRef]
45. Ludwig, R. Water: From Clusters to the Bulk. *Angew. Chem. Int. Ed.* **2001**, *40*, 1808–1827. [CrossRef]
46. Keutsch, F.N.; Saykally, R.J. Water clusters: Untangling the mysteries of the liquid, one molecule at a time. *Proc. Natl. Acad. Sci. USA* **2001**, *98*, 10533–10540. [CrossRef]
47. Dunn, M.E.; Pokon, E.K.; Shields, G.C. The ability of the Gaussian-2, Gaussian-3, Complete Basis Set–QB3, and Complete Basis Set–APNO model chemistries to model the geometries of small water clusters. *Int. J. Quantum Chem.* **2004**, *100*, 1065–1070. [CrossRef]
48. Shields, R.M.; Temelso, B.; Archer, K.A.; Morrell, T.E.; Shields, G.C. Accurate Predictions of Water Cluster Formation, $(H_2O)_{n=2-10}$. *J. Phys. Chem. A* **2010**, *114*, 11725–11737. [CrossRef]
49. Klots, A.R.; Newaz, A.K.M.; Wang, B.; Prasai, D.; Krzyzanowska, H.; Lin, J.; Caudel, D.; Ghimire, N.J.; Yan, J.; Ivanov, B.L.; et al. Probing excitonic states in suspended two-dimensional semiconductors by photocurrent spectroscopy. *Sci. Rep.* **2014**, *4*, 6608. [CrossRef]
50. Yu, H.; Cui, X.; Xu, X.; Yao, W. Valley excitons in two-dimensional semiconductors. *Natl. Sci. Rev.* **2015**, *2*, 57–70. [CrossRef]
51. Mouri, S.; Miyauchi, Y.; Matsuda, K. Tunable Photoluminescence of Monolayer MoS_2 via Chemical Doping. *Nano Lett.* **2013**, *13*, 5944–5948. [CrossRef] [PubMed]
52. Tongay, S.; Zhou, J.; Ataca, C.; Liu, J.; Kang, J.S.; Matthews, T.S.; You, L.; Li, J.; Grossman, J.C.; Wu, J. Broad-Range Modulation of Light Emission in Two-Dimensional Semiconductors by Molecular Physisorption Gating. *Nano Lett.* **2013**, *13*, 2831–2836. [CrossRef] [PubMed]

Disclaimer/Publisher's Note: The statements, opinions and data contained in all publications are solely those of the individual author(s) and contributor(s) and not of MDPI and/or the editor(s). MDPI and/or the editor(s) disclaim responsibility for any injury to people or property resulting from any ideas, methods, instructions or products referred to in the content.